COMMUNICATION

Check for updates

Preparation and application of piperidinium-functionalized cross-linked polynorbornene-based anion-exchange membranes

Haixia Zhang,†[a,b] Yubing Xiao,†[a,b] Hesong Guo,[c] Xiang Li,[c] Yu Wang [ID] *[a] and Wei You [ID] *[a,b]

Anion-exchange membranes (AEMs) with cross-linked vinyl-addition polynorbornene (VA-PNB) backbones have proved to be outstanding candidates for water electrolysis due to their high hydroxide conductivity and alkaline stability. Herein, we introduced piperidinium cations into the VA-PNB network to produce high performance AEMs (D-2-Pip) through a simple fabrication process. The resulting membrane exhibited a desirable combination of mechanical robustness, high-dimensional stability (swelling ratio of 24%), and remarkable hydroxide conductivity (138 mS cm^{-1} at 80 °C). It demonstrated exceptional alkaline stability, retaining over 98% of its initial conductivity after 1320 hours in 1 M KOH at 80 °C. The membrane was successfully applied in anion-exchange membrane water electrolyzers (AEMWEs), achieving a high current density of 1.93 A cm^{-2} at 2.0 V and outstanding operational durability for over 1400 hours. This study demonstrates the promising potential of the D-2-Pip AEM for efficient and stable clean energy conversion applications.

Introduction

The intensifying global energy crisis and environmental challenges urgently demand innovative strategies for clean and efficient energy storage.[1–4] Within this context, hydrogen has emerged as a leading next-generation energy carrier due to its exceptional gravimetric energy density, renewability, and near-zero-emission combustion profile. Producing high-purity hydrogen *via* water electrolysis constitutes a critical technological pathway toward a hydrogen economy, garnering significant research attention in recent years.[5–8] In electrochemical systems, particularly anion-exchange membrane water electrolyzers (AEMWEs) and anion-exchange membrane fuel cells (AEMFCs),[9–13] AEMs serve as indispensable components. Their fundamental roles include: (i) physically separating anode/cathode compartments and (ii) selectively facilitating hydroxide ion (OH$^-$) conduction.[14] The overall AEM performance (encompassing ionic conductivity, alkaline stability, and mechanical robustness) directly governs the energy efficiency, long-term operational durability, and cost-effectiveness of the entire energy conversion system. Consequently, developing high-performance AEMs is paramount for enabling scalable deployment and sustainable advancement of hydrogen technologies.

In recent years, the field of AEMs has witnessed remarkable advancements. However, there are still several critical bottlenecks that must be overcome before their practical application can be realized. Traditional aromatic polymer-based materials for AEMs exhibit good chemical corrosion resistance. However, their inherent molecular chain rigidity often limits the mobility of the ion-conducting groups, resulting in membranes with low ionic conductivity. More seriously, such materials are usually prepared using super acids (*e.g.* trifluoromethanesulfonic acid) as solvents, raising additional environmental and corrosion concerns.[15–18] On the other hand, AEM materials with polyolefin backbones[19] have shown potential in enhancing ion conduction performance.[20–24] Nonetheless, their mechanical properties (such as anti-swelling capability and toughness) and long-term chemical endurance in harsh electrochemical settings often fall short of the demands of practical devices.[25–29] Consequently, developing and designing novel AEM material systems that can simultaneously achieve high hydroxide-ion conductivity, excellent chemical stability, robust mechanical properties, and precisely regulated water absorption and swelling behavior has become the current core scientific objective and key technological challenge in this field.

Among AEM materials with diverse polyolefin backbones, vinyl-addition polynorbornene (VA-PNB) shows outstanding performance mostly due to its high glass transition temperature (T_g) and high chemical and mechanical stability, and ease of synthesis.[30] To control the swelling properties, bis-

[a] Beijing National Laboratory for Molecular Sciences (BNLMS), CAS Key Laboratory of Engineering Plastics, Institute of Chemistry, Chinese Academy of Sciences, Beijing, 100190, China. E-mail: weiyou@iccas.ac.cn, ywang507@iccas.ac.cn
[b] University of Chinese Academy of Sciences, Beijing 100049, China
[c] Beijing Cleanway Technology Co., Ltd, Beijing 102611, China
† These authors contributed equally to this work.

amine[31,32] and dithiol cross-linkers[33,34] are commonly introduced to produce cross-linked VA-PNB-based AEMs. Building on our group's prior work,[35,36] AEMs (**D-2-H**) prepared from a commercial dicyclopentadiene (DCPD) comonomer, dithiol for photo-induced *in situ* cross-linking, and alkyl-trimethylammonium (TMA) to provide cationic groups retain functionality under high-temperature and highly alkaline conditions. Numerous reports have proposed that cyclic piperidinium cations have alkaline stability superior to that of TMA, especially when attached to flexible alkyl side chains.[37–40] Therefore, we herein propose a straightforward post-polymerization functionalization approach to install piperidinium cations into dithiol-cross-linked VA-PNB AEMs. In comparison with previously reported bis-piperidinium-cross-linked VA-PNB AEMs reported by Chen and coworkers,[41] our ionization approach in aqueous media proceeds under mild reaction conditions and exhibits rapid transformation, and thus holds promise for potential scale-up. More importantly, this material system achieves simultaneous enhancements in alkaline stability, mechanical flexibility, and AEMWE device durability.

Experimental section

Materials

1,10-Decanedithiol, phenylbis(2,4,6-trimethylbenzoyl)phosphine oxide (PI 819), chlorobenzene, and 1-methylpiperidine were purchased from Energy Chemical Co., Shanghai, China. CLi-01 ionomer solution was provided by Beijing Cleanway Technology Co., Ltd. All abovementioned chemicals were used as received without further purification.

Dicyclopentadiene (DCPD) was purchased from Energy Chemical Co., Shanghai, China, and purified by vacuum transfer prior to use. Alkyl-bromide-functionalized norbornene (BrNB)[42] was synthesized according to the literature procedures.

Fabrication of a D-2-Pip AEM. To fabricate a D-2 AEM, the D-2 copolymer (6.1 g, 32.6 mmol, prepared according to the literature procedure[35]) was first dissolved in chlorobenzene (25 mL) together with 1,10-decanedithiol (1.44 mL, 6.5 mmol) and PI 819 (201 mg, 0.48 mmol). Upon reaching a suitable viscosity, the solution was uniformly doctor-bladed onto a clean glass plate to form a thin film (D-2 AEM). Subsequently, the film was irradiated under UV light (365 nm) for 1 h to perform the cross-linking reaction while solvent-casting. Following cross-linking, the film was placed in an 80 °C environment to allow complete evaporation of the chlorobenzene solvent, yielding a uniform D-2 cross-linked membrane. Finally, the D-2 cross-linked membrane was immersed in 1-methylpiperidine aqueous solution (5 vol%) and treated at 80 °C for 2 h to achieve piperidinium functionalization, successfully producing the piperidinium-functionalized AEM (**D-2-Pip** AEM).

See the SI for more details about the synthesis of the D-2 copolymer, membrane characterization, and AEM water electrolysis device assembly.

Results and discussion

Polymer D-2 was synthesized *via* addition polymerization and characterized by NMR spectroscopy. As shown in Fig. S1, the integration ratio between the signal at 5.66 ppm (corresponding to the alkene bond of DCPD) and the signal at 3.42 ppm (corresponding to the C–Br bond) is 1 : 2. This result confirms the successful synthesis of copolymer D-2. The reactive casting with UV-induced dithiol cross-linking was performed according to the literature procedures.[35] Subsequently, the membranes were immersed in 1-methylpiperidine solution for piperidinium functionalization (Scheme 1). In our previous attempt to install TMA groups on the VA-PNB membranes, the membrane needs to be soaked in trimethylamine aqueous solution for over 48 hours. Due to the low boiling point of trimethylamine, heating would decrease the solubility of trimethylamine in water and ultimately lead to decreased quaternization efficiency. In contrast, the 1-methylpiperidine has a much higher boiling point (106–107 °C under atmospheric pressure), so that the quaternization process can be performed at elevated temperature for acceleration. Various piperidine concentrations and reaction times were tried (Table S1), and it was revealed that the quaternization reached over 80% conversion (evaluated based on the ion-exchange capacity (IEC) calculation given in Table 1) at 80 °C for 2 hours with the use of aqueous 1-methylpiperidine solution at a concentration as low as 5 vol%. X-ray photoelectron spectroscopy (XPS) analysis of the sample surface after ion exchange also indicated incomplete quaternization (Table S3). Complete quaternization might have been achieved when the reaction time was extended to 12 hours, but the membranes became overswollen and fragile during sequential anion exchange and testing. Therefore, the quaternization condition was set at 80 °C for 2 hours, ensuring high functionalization efficiency.

FT-IR characterization of the resulting **D-2-Pip** AEM confirmed successful piperidinium functionalization. As shown in Fig. 1(a), the emergence of a characteristic CH$_3$–N$^+$ band at 1456 cm^{-1} in the FT-IR spectrum corroborates the quaternization of the piperidinium moiety in the cross-linked **D-2-Pip** AEM. Subsequently, a comprehensive investigation of its microstructure, electrochemical properties, and device-level performance was undertaken.

As shown in Scheme 1, the **D-2-Pip** AEM treated with piperidine ionization exhibits a smooth surface without obvious defects. This surface characteristic indicates homogeneous film-forming during both reactive casting and quaternization. To further investigate the microstructural features, we performed detailed characterization studies using scanning electron microscopy (SEM). As shown in Fig. 2, both the surface and cross-section of the **D-2-Pip** AEM present a dense and pore-free structure.

In this study, small-angle X-ray scattering (SAXS) was employed to investigate the effect of hydration on the microstructure of D-2 membranes and **D-2-Pip** AEMs. As shown in Fig. 1(b), the one-dimensional SAXS profile of the dry D-2 membrane exhibited no distinct peaks, indicating the
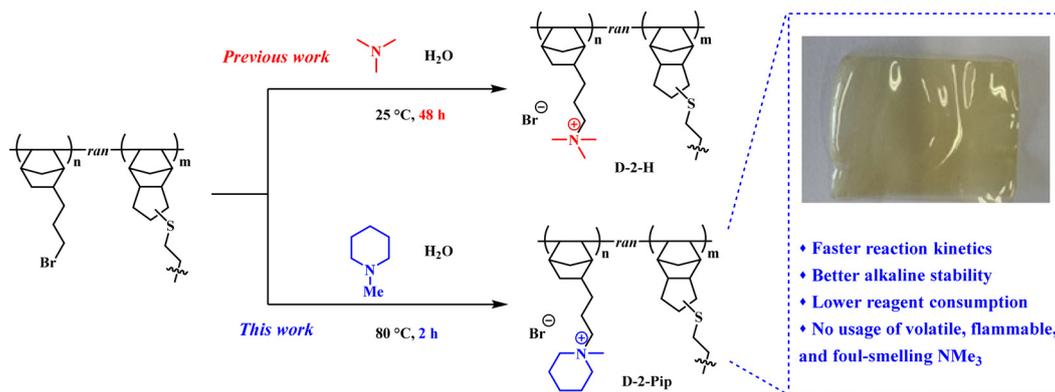
Scheme 1 Illustration of the synthesis of **D-2-Pip** and its comparison with **D-2-H**.

**Table 1** Properties of the **D-2-Pip** AEM and its comparison with TMA-functionalized **D-2-H** [35]

	D-2-Pip	D-2-H [35]
WU[a] (%)	72	51
SR[b] (%)	15	11
IEC$_{theo}$ (mmol Cl$^-$ g^{-1})	2.63	2.88
IEC[c] (mmol Cl$^-$ g^{-1})	2.08	2.75
σ^d (HCO$_3^-$, mS cm^{-1}) at 25 °C	13.6	14.2
σ^e (OH$^-$, mS cm^{-1}) at 80 °C	138	195
Conductivity retention after 1 M KOH treatment at 80 °C	98% after 1320 hours	83% after 1200 hours

^{a} Water uptake at 25 °C = 100 × [mass$_{wet}$ − mass$_{dry}$]/mass$_{dry}$%. ^{b} Dimensional change at 25 °C = 100 × [length$_{wet}$ − length$_{dry}$]/length$_{dry}$%. ^{c} IEC was determined by Mohr's titration. ^{d} Measured in bulk water. ^{e} Measured under >98% RH.

absence of long-range ordered structures (*e.g.*, hydrophilic/hydrophobic domains) in the material. Similarly, no scattering peaks were observed for the hydrated D-2-aqueous membrane. However, compared with the dry membrane, its scattering intensity in the high-q region was significantly enhanced and remained nearly constant with increasing q. This suggests that hydration promotes local electron-density fluctuations but is insufficient to induce long-range ordering. Likewise, no scattering peaks were detected for either the dry or hydrated **D-2-Pip** membranes. Therefore, all D-2 and **D-2-Pip** membranes studied here lack long-range ordered microstructures. The obtained SAXS results are consistent with the analysis of TEM images (Fig. S3). A comparison between SAXS plots of ammonium-based **D-2-H** [35] and piperidinium-based **D-2-Pip** in the dry state reveals that only the former exhibits a nearly constant scattering intensity across the q range of 0.05–0.18 Å^{-1}, whereas the latter shows a decreasing trend with increasing q. Previous studies on cross-linked rubber systems have indicated that elevated cross-link densities restrict molecular chain mobility,[43] leading to reduced electron density inhomogeneities that manifest as a plateau (rather than a decrease) in SAXS intensity with increasing q. Consequently, the observed electron density inhomogeneities in **D-2-Pip** AEMs indicate greater molecular chain flexibility compared to **D-2-H**. At the
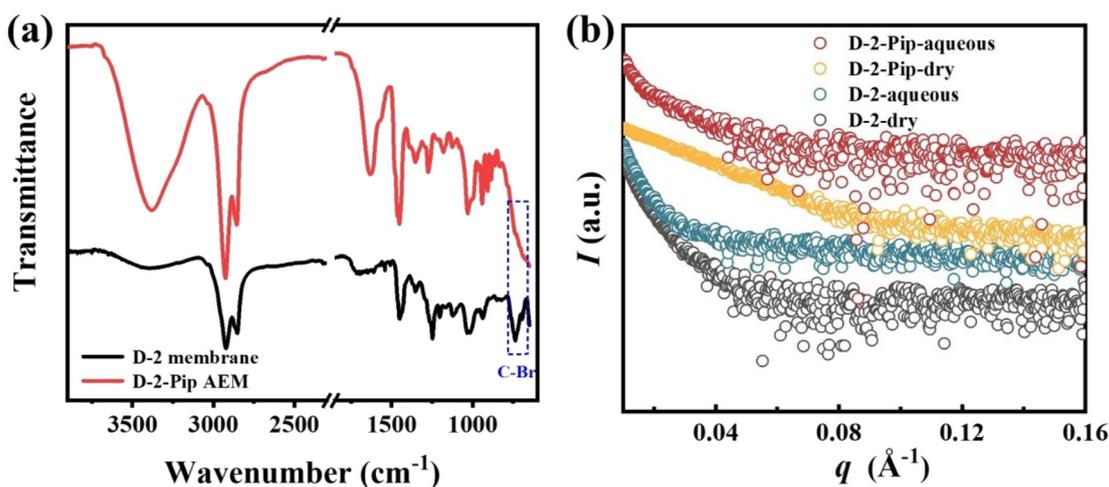
Fig. 1 (a) The FT-IR comparison of the D-2 membrane and **D-2-Pip** AEM. (b) Comparisons of 1-D SAXS profiles under aqueous or dry conditions for D-2 membranes and **D-2-Pip** AEMs. The plots are vertically shifted to avoid overlapping.
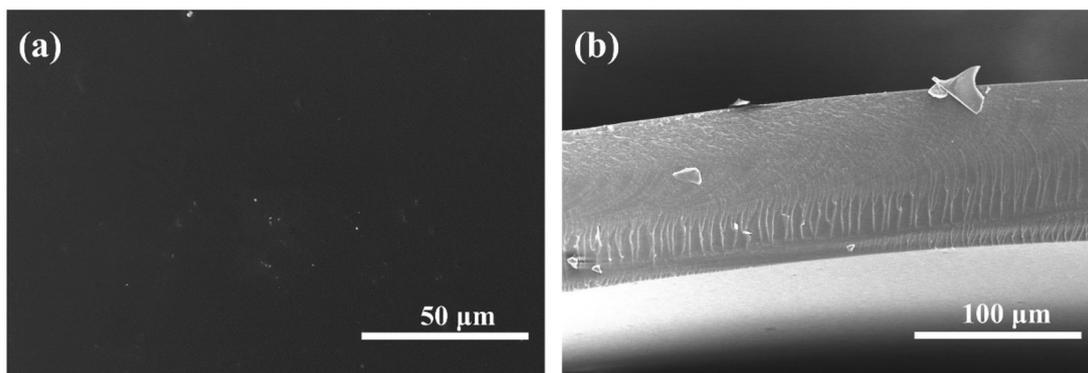
Fig. 2 Surficial SEM (a) and cross-sectional SEM (b) images of **D-2-Pip**.

microscopic level, this enhanced chain mobility promotes ion transport, thereby contributing to improved AEM performance.

To thoroughly explore the potential application of **D-2-Pip** AEMs in electrochemical energy conversion devices, a comprehensive and systematic investigation of their physicochemical properties was conducted (Table 1). The properties of TMA-functionalized **D-2-H** were also listed to compare the difference of two different cationic functional groups.[35] First, the water uptake (WU) and swelling ratio (SR) of **D-2-Pip** AEMs were evaluated. The results show that the WU of **D-2-Pip** at 25 °C is only 72%, with minimal change as the temperature increases, reaching only 83% even at 80 °C (Fig. 3a). In the SR tests, we observed that the SR value at 25 °C is merely 15%, and it

increases only slightly with temperature, reaching 20% at 80 °C (Fig. 3b). These findings indicate that **D-2-Pip** AEMs not only possess hygroscopic properties but also exhibit excellent dimensional stability. However, when compared with **D-2-H** membranes (Table 1), it was noted that membranes functionalized with piperidinium cations exhibit higher values in both WU and SR. This may be attributed to the larger size of the piperidinium cations, which results in less tightly packed polymer backbones compared to that in **D-2-H** membranes.

In the IEC test, the **D-2-Pip** AEM demonstrated an IEC value of 2.08 mmol Cl^- g^{-1}. The higher molar mass of the piperidinium cation rendered a lower IEC than its alkyltrimethylammonium cation counterpart in **D-2-H**. The degree of quaternization achieved 80% according to the IEC/IEC_{theo} ratio. This
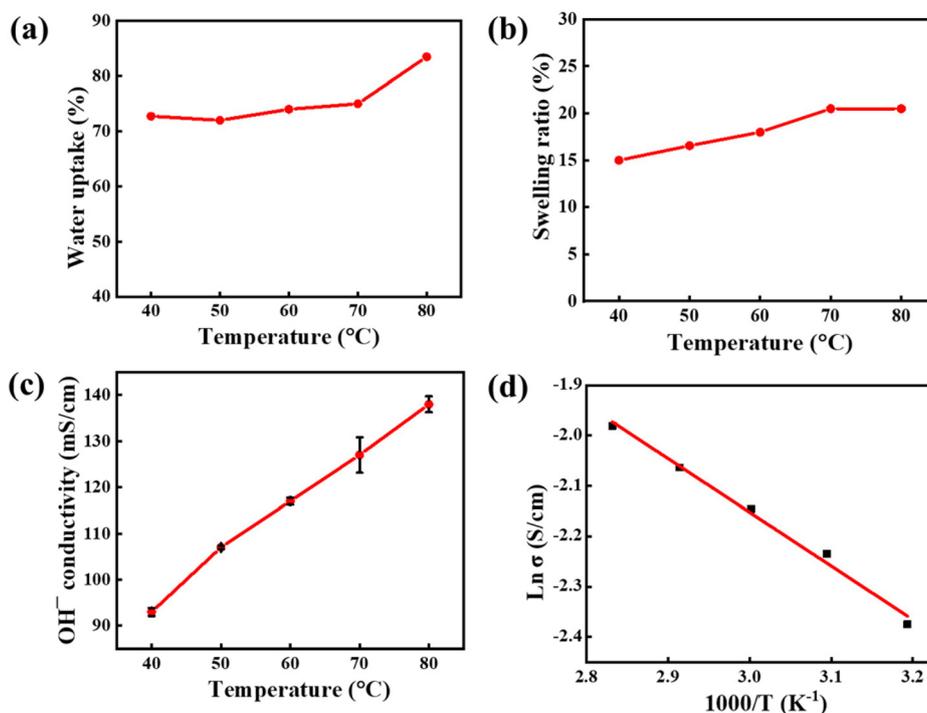

Fig. 3 (a) Water uptake, (b) swelling ratio, (c) hydroxide conductivity, and (d) Arrhenius plots of the **D-2-Pip** AEM at various temperatures.

number is consistent with the quaternization reaction time optimization shown in Table S1. As indicated by the SR results, the IEC of 2.08 mmol Cl$^-$ g^{-1} did not lead to excessive swelling, demonstrating that the membrane maintains dimensional stability while exhibiting efficient ion-transport capability. These findings collectively highlight the excellent physicochemical properties of the **D-2-Pip** AEM and its potential for practical applications.

Furthermore, considering that the high OH$^-$ conductivity of AEMs is a key factor in enhancing the current density of AEMWEs, we measured the "true OH$^-$ conductivity" of AEMs at different temperatures under direct current and high humidity conditions (relative humidity RH > 98%) using an *in situ* decarbonation method. Owing to the high WU of **D-2-Pip** AEMs, their Br$^-$ conductivity at 25 °C reached 12.5 mS cm^{-1} and their HCO$_3^-$ conductivity was 13.6 mS cm^{-1} (Table 1). This result preliminarily demonstrated the high efficiency of **D-2-Pip** AEMs in ionic transport. Their OH$^-$ conductivity at higher temperatures showed that at 80 °C the OH$^-$ conductivity significantly increased to 138 mS cm^{-1}. This excellent conductivity performance not only proved the superior ionic transport efficiency of **D-2-Pip** AEMs but also indicated that they could maintain high ionic conductivity even at elevated temperatures[44] (Fig. 3c and Fig. S2). Furthermore, calculations revealed that the activation energy of **D-2-Pip** is only 8.86 kJ mol^{-1} (Fig. 3d), which is lower than the values of **D-2-H** and other AEMs.[31,35,45]

The mechanical properties under humid conditions are crucial for practical applications. Therefore, we conducted tensile stress–strain tests on a **D-2-Pip** AEM after aqueous treatment. The results showed that the tensile strength of this AEM was 9 MPa, with a corresponding elongation at break of up to 38% (Fig. 4a and Table S2). Although the tensile strength of the **D-2-Pip** AEM is lower than that of the previous dry norbornene-based AEMs,[35] its high elongation at break is a significant advantage. The high elongation at break indicates that the membrane can withstand considerable deformation under external forces without breaking, which implies better flexibility and fatigue resistance in practical applications. The trend where piperidinium-functionalized VA-PNB AEMs are more flexible than TMA-functionalized membranes was consistent with our previous report on a semi-interpenetrated network.[36] This characteristic enables **D-2-Pip** AEMs to adapt to mechanical stress variations during the water electrolysis process, reducing the risk of membrane rupture due to brittleness, and thereby enhancing the stability and service life of the system. To highlight the conductivity–flexibility balance, a comparison with other piperidinium-based AEMs from the recent literature is presented in Table S2. The di-piperidinium-cross-linked *x*-PFTP-DP-C10-10 reported by Chen *et al.* exhibi-
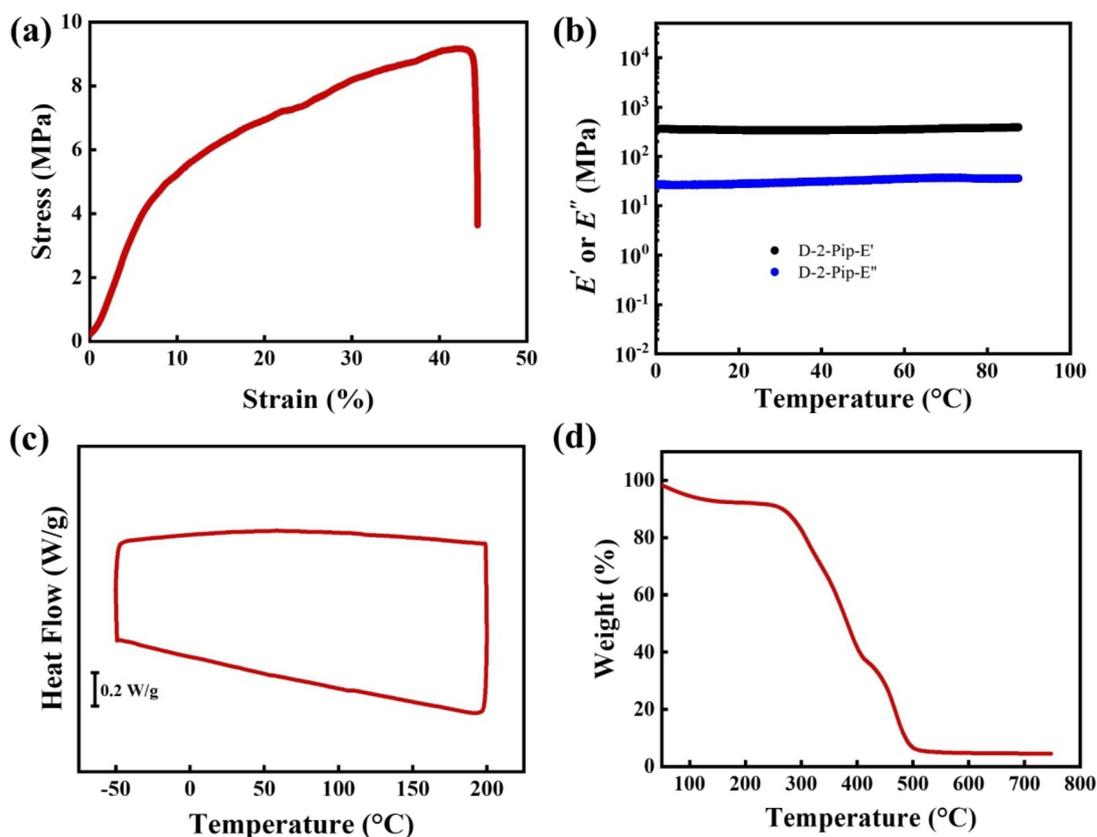

Fig. 4 (a) Stress–strain, (b) DMA, (c) DSC and (d) TGA traces of the **D-2-Pip** AEM.

ted high tensile strength (~86 MPa) and moderate elongation at break (~34%) with excellent hydroxide conductivity (~165 mS cm^{-1}).[46] Notably, Wu *et al.* reported fluorinated poly (aryl piperidinium) (FPAP) membranes with an exceptional combination of high conductivity (~150 mS cm^{-1}) and superior mechanical flexibility (elongation at break >40%).[47] Strikingly, our **D-2-Pip** membrane demonstrates a comparable elongation at break (38%) to the fluorinated FPAP membrane while maintaining competitive ionic conductivity, representing an excellent conductivity–flexibility balance without the need for fluorination or complex cross-linking strategies.

To further validate these findings, we conducted DMA tests on **D-2-Pip** (Fig. 4b). Since the operating temperature of the device is below 80 °C, the testing range was also limited to below 80 °C. The results showed that both the storage modulus (E') and loss modulus (E'') exhibited minimal variation within the 0–90 °C range, demonstrating that temperature has little effect on the mechanical properties of the membrane. Therefore, modifying the structure and properties of the cations to regulate the mechanical properties of AEMs can not only optimize their elongation at break but also significantly improve their reliability and durability in practical applications.

In DSC testing (Fig. 4c), **D-2-Pip** AEMs showed no significant signals related to phase transitions within the 0–200 °C range. Given that AEMWEs typically operate at a temperature of 60 °C or 80 °C, the thermal stability of AEMs is critical. Therefore, we conducted thermogravimetric analysis (TGA) tests on **D-2-Pip** AEMs to evaluate their thermal stability. The TGA results showed (Fig. 4d) that after the initial mass loss due to water evaporation at around 100 °C, the mass loss of **D-2-Pip** AEMs mainly occurred in three stages: the first stage occurred at approximately 308 °C, attributed to the degradation of the piperidinium group; the second stage occurred at around 380 °C, which is speculated to be due to the degradation of the part where the thiol and alkene groups undergo click reactions; and the third stage occurred at approximately 470 °C, likely resulting from the degradation of the norbornene framework. Crucially, no significant degradation was observed for **D-2-Pip** AEMs below 300 °C. This result indicates that **D-2-Pip** AEMs possess excellent thermal stability, which can easily meet the operational requirements of AEMWEs at high temperatures.

In alkaline energy devices, AEMs serve as a core component, and their performance directly determines the operational efficiency and service life of the entire system. Therefore, alkaline stability is one of the key indicators for evaluating the performance of AEMs. AEMs with excellent alkaline stability can maintain stable ionic conductivity over long-term operation, thereby significantly enhancing the service life and operational efficiency of AEMWE systems. To thoroughly assess their alkaline stability, **D-2-Pip** AEMs were immersed in 1 M KOH solution at 80 °C and their HCO$_3^-$ conductivities were periodically monitored. As shown in Fig. 5, after 1320 hours of alkaline stability testing, the bicarbonate ion conductivity of the **D-2-Pip** AEM remained virtually
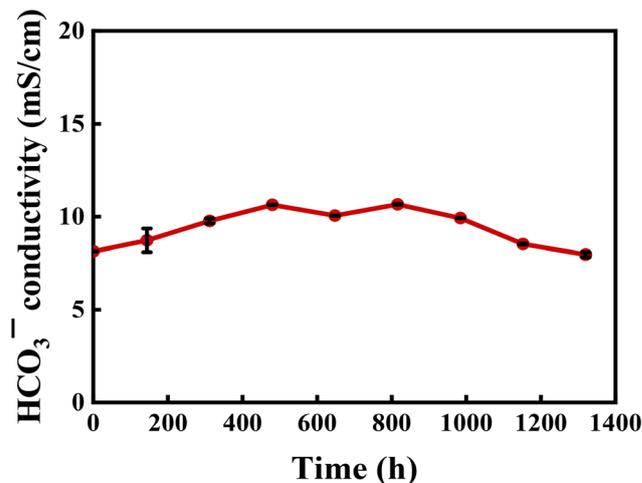

**Fig. 5** The alkaline stability of the **D-2-Pip** AEM.

unchanged. It outperformed the **D-2-H** AEM, which retained 83% ionic conductivity after the same alkaline treatment.[35] This result indicates that the **D-2-Pip** AEM possesses excellent chemical stability and structural integrity in alkaline environments. Even under long-term highly alkaline conditions, the membrane can still maintain highly efficient ionic conductivity, which provides strong support for its practical application in AEMWEs.

In this study, AEMWEs were assembled using the **D-2-Pip** AEM, and its performance was systematically evaluated. To achieve efficient electrolysis, CAPist-L1 was used as the oxygen evolution reaction (OER) catalyst layer,[48] while Pt/C electrocatalysts combined with a polynorbornene-based CLi-01 ionomer on carbon paper were fabricated as the hydrogen evolution reaction (HER) layer. Polarization performance was evaluated under varying alkaline concentrations and temperatures. Initially, the water electrolysis performance was compared at a constant temperature (60 °C) with KOH concentrations of 0.1 M, 0.5 M, and 1 M (Fig. 6a). The increase in alkaline concentration led to higher current densities at lower voltages. At 60 °C in 1 M KOH, the membrane electrode assembly based on **D-2-Pip** achieved current densities of 1.11 A cm^{-2} and 1.93 A cm^{-2} at voltages of 1.8 V and 2.0 V, respectively. Subsequently, polarization curves were measured at a fixed KOH concentration (1 M) and temperatures of 40 °C, 60 °C, and 80 °C (Fig. 6b). Although increasing the temperature improved the device performance, the polarization characteristics at 60 °C and 80 °C were found to be similar. Therefore, 60 °C and 1 M KOH were determined to be the optimal test conditions. Additionally, a durability test lasting 1407 h was performed under conditions of 60 °C, 1 M KOH electrolyte and a constant current density of 1 A cm^{-2} (Fig. 6c). The results, after an initial stabilization period of 200 hours, revealed that the voltage increase rate of the electrolyzer was extremely low from 200 h to 1407 h, changing from 1.9869 V to 1.9806 V. In comparison, the **D-2-H** AEM exhibited a voltage degradation rate of 2.845 mV h^{-1} after 500 h of operation under milder conditions (500 mA cm^{-2}, 60 °C, 0.1 M KOH).[35] These excellent long-term
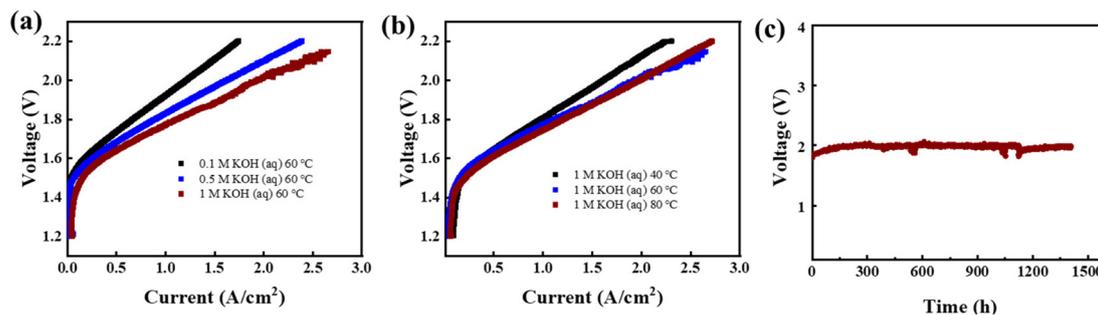
Fig. 6 (a) Polarization curves for **D-2-Pip** at 60 °C in 0.1 M, 0.5 M or 1 M KOH as part of the water electrolyzer. (b) Polarization curves for **D-2-Pip** in 1 M KOH at 40 °C, 60 °C or 80 °C as part of the water electrolyzer. (c) Durability test of **D-2-Pip** at 60 °C in 1 M KOH aqueous solution operating in galvanic mode at 1 A cm^{-2} (with a nickel–iron-based electrocatalyst (CAPist-L1) as the anode and Pt/C on carbon paper as the cathode).
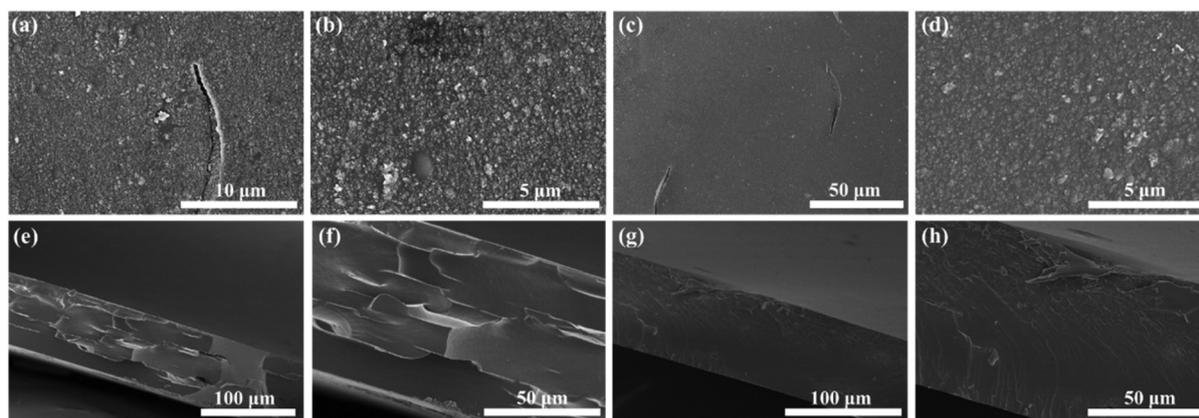
Fig. 7 SEM images of **D-2-Pip** after the durability test of 330 h: (a and b) surface of the dark region, (c and d) surface of the light region, (e and f) cross-section of the dark region, and (g and h) cross-section of the light region, all at various magnifications.

operational stability results of **D-2-Pip** AEMs fully demonstrated the improvement of membrane durability by incorporating piperidinium cations onto cross-linked VA-PNB backbones.

A water electrolyzer after a durability test of 330 h was disassembled to evaluate the status of the membrane. It was found that the surface of the membrane had dark regions and light regions, likely caused by the residual electrocatalyst. As revealed by the images of the SEM analysis in Fig. 7, the darker region appeared more heterogeneous and to have a rougher surface (Fig. 7a–d). In the cross-sectional images, the dark region exhibited an uneven fractured surface after liquid nitrogen breaking (Fig. 7e and f), whereas the light region showed a morphology more similar to that of the pristine **D-2-Pip** AEM (Fig. 7g and h, compared with Fig. 2b). These results reveal that although the membrane retained its integrity and dense structures after the durability study, the regional aging of the material may vary depending on the interaction with electrocatalysts. Further investigation will focus on the interfacial structures and stability of the membranes, ionomers, and electrocatalysts in polynorborene-membrane-based water electrolyzers.

Conclusion

In summary, a novel piperidinium and polynorbornene-based AEM was developed that effectively balances alkaline stability and high conductivity—a key challenge in AEMWEs. The combination of piperidinium cations and dithiol-cross-linked VA-PNB backbones is easily achieved by aqueous membrane soaking for only 2 hours, and the resultant membrane demonstrates good dimensional stability and mechanical strength under wet conditions, along with high hydroxide conductivity (138 mS cm^{-1} at 80 °C). More importantly, it exhibits exceptional durability, with nearly complete conductivity retention after 1320 hours in 1 M KOH at 80 °C. When applied in AEMWEs, the membrane enables high current density (1.93 A cm^{-2} at 2.0 V) and minimal voltage decay under continuous operation for 1407 hours. These results underscore the strong potential of the **D-2-Pip** AEM for industrial hydrogen production applications. This design strategy can be extended to other cyclic cationic systems and diverse rigid polymer backbones. By tuning the cationic structure and backbone rigidity, synergistic optimization of membrane stability and conduc-

tivity can be achieved, thereby providing a versatile design approach for material innovation toward next-generation electrochemical energy devices with high efficiency and long operational lifetimes.

Conflicts of interest

The authors declare the following financial interests/personal relationships which may be considered as potential competing interests: Wei You and Yu Wang are scientific co-founders of Beijing Cleanway Technology Co., Ltd., supplier of CLi-01 ionomer solution. Hesong Guo and Xiang Li are employees of Beijing Cleanway Technology Co., Ltd. Other authors declare that they have no known competing financial interests or personal relationships that could have appeared to influence the work reported in this paper.

Data availability

The data supporting this article have been included as part of the supplementary information (SI). The influence of different piperidine concentrations and reaction times on conductivity of D-2-pip membranes; Performance comparison between D-2-Pip AEM and other membranes; The XPS of D-2-Pip AEM; The 1H NMR of D-2; Hydroxide conductivities of D-2-Pip AEM; TEM images of D-2-Pip membranes. See DOI: https://doi.org/10.1039/d6lp00002a.

Acknowledgements

References

1 Y. Yang, P. Li, X. Zheng, W. Sun, S. X. Dou, T. Ma and H. Pan, *Chem. Soc. Rev.*, 2022, **51**, 9620–9693.

2 D. R. Dekel, *J. Power Sources*, 2018, **375**, 158–169.

3 C. Pierucci, L. Paleari, J. Baker, C. C. M. Sproncken, M. Folkesson, J. P. Wesseler, A. Vracar, A. Dodero, F. Nanni, J. A. Berrocal, M. Mayer and A. Ianiro, *RSC Appl. Polym.*, 2025, **3**, 209–221.

4 R. P. S, V. Prasannavenkadesan, V. Katiyar and A. S. Achalkumar, *RSC Appl. Polym.*, 2025, **3**, 499–531.

5 X. Zou and Y. Zhang, *Chem. Soc. Rev.*, 2015, **44**, 5148–5180.

6 G. Zhao, K. Rui, S. X. Dou and W. Sun, *Adv. Funct. Mater.*, 2018, **28**, 1803291.

7 Z. F. Pan, L. An, T. S. Zhao and Z. K. Tang, *Prog. Energy Combust. Sci.*, 2018, **66**, 141–175.

8 S. Zhang, W. Ma, L. Tian, D. Kong, Q. Zhu, F. Wang and H. Zhu, *ACS Appl. Mater. Interfaces*, 2024, **16**, 7660–7669.

9 M. Alesker, M. Page, M. Shviro, Y. Paska, G. Gershinsky, D. R. Dekel and D. Zitoun, *J. Power Sources*, 2016, **304**, 332–339.

10 E. M. Sommer, L. S. Martins, J. V. C. Vargas, J. E. F. C. Gardolinski, J. C. Ordonez and C. E. B. Marino, *J. Power Sources*, 2012, **213**, 16–30.

11 M. Piana, M. Boccia, A. Filpi, E. Flammia, H. A. Miller, M. Orsini, F. Salusti, S. Santiccioli, F. Ciardelli and A. Pucci, *J. Power Sources*, 2010, **195**, 5875–5881.

12 H. Deng, D. Wang, X. Xie, Y. Zhou, Y. Yin, Q. Du and K. Jiao, *Renewable Energy*, 2016, **91**, 166–177.

13 D. S. Kim, A. Labouriau, M. D. Guiver and Y. S. Kim, *Chem. Mater.*, 2011, **23**, 3795–3797.

14 Y. J. Wang, J. Qiao, R. Baker and J. Zhang, *Chem. Soc. Rev.*, 2013, **42**, 5768–5787.

15 J. Wang, Y. Zhao, B. P. Setzler, S. Rojas-Carbonell, C. B. Yehuda, A. Amel, M. Page, L. Wang, K. Hu, L. Shi, S. Gottesfeld, B. Xu and Y. Yan, *Nat. Energy*, 2019, **4**, 392–398.

16 J. Huang, Z. Yu, J. Tang, P. Wang, Q. Tan, J. Wang and X. Lei, *Int. J. Hydrogen Energy*, 2022, **47**, 27800–27820.

17 C. Long, Z. Wang and H. Zhu, *Int. J. Hydrogen Energy*, 2021, **46**, 18524–18533.

18 W. Song, X. Ge, L. Wu, Z. Yang and T. Xu, *Joule*, 2025, **9**, 102051.

19 B. Zhong, Y. Zhang, W. You and Y. Wang, *RSC Appl. Polym.*, 2025, **3**, 97–110.

20 Q.-R. Lu and W. You, *Acta. Polym. Sin.*, 2020, **51**, 1140–1146.

21 L. Zhu, X. Yu, X. Peng, T. J. Zimudzi, N. Saikia, M. T. Kwasny, S. Song, D. I. Kushner, Z. Fu, G. N. Tew, W. E. Mustain, M. A. Yandrasits and M. A. Hickner, *Macromolecules*, 2019, **52**, 4030–4041.

22 J. Han, C. Liu, Y. Lu, X. Zheng, W. Li, Y. Liu, X. Yang, Z. Ren, M. Hu, L. Xiao and L. Zhuang, *Polymer*, 2023, **285**, 126377.

23 C. R. Peltier, W. You, D. F. Volcanjk, Q. Li, A. J. Macbeth, H. D. Abruña and G. W. Coates, *ACS Energy Lett.*, 2023, **8**, 2365–2372.

24 S. A. Franklin, C. Crean and J. R. Varcoe, *RSC Appl. Polym.*, 2026, **4**, 320–327.

25 Y. Ye, K. K. Stokes, F. L. Beyer and Y. A. Elabd, *J. Membr. Sci.*, 2013, **443**, 93–99.

26 P. Cotanda, G. Sudre, M. A. Modestino, X. C. Chen and N. P. Balsara, *Macromolecules*, 2014, **47**, 7540–7547.

27 K. J. Noonan, K. M. Hugar, H. A. T. Kostalik, E. B. Lobkovsky, H. D. Abruna and G. W. Coates, *J. Am. Chem. Soc.*, 2012, **134**, 18161–18164.

28 C. T. Womble, G. W. Coates, K. Matyjaszewski and K. J. T. Noonan, *ACS Macro Lett.*, 2016, **5**, 253–257.

29 T. Zhu, Y. Sha, H. A. Firouzjaie, X. Peng, Y. Cha, D. Dissanayake, M. D. Smith, A. K. Vannucci, W. E. Mustain and C. Tang, *J. Am. Chem. Soc.*, 2020, **142**, 1083–1089.

30 M. V. Bermeshev and P. P. Chapala, *Prog. Polym. Sci.*, 2018, **84**, 1–46.

31 M. Mandal, G. Huang and P. A. Kohl, *ACS Appl. Energy Mater.*, 2019, **2**, 2447–2457.

32 M. Mandal, G. Huang, N. U. Hassan, W. E. Mustain and P. A. Kohl, *J. Mater. Chem. A*, 2020, **8**, 17568–17578.

33 W. Yang, J. Chen, J. Yan, S. Liu, Y. Yan and Q. Zhang, *J. Polym. Sci.*, 2022, **60**, 627–649.

34 L. Zhu, T. J. Zimudzi, N. Li, J. Pan, B. Lin and M. A. Hickner, *Polym. Chem.*, 2016, **7**, 2464–2475.

35 T. Wang, Y. Wang and W. You, *J. Membr. Sci.*, 2024, **702**, 122747.

36 T. Wang, Y. Wang and W. You, *Chin. J. Polym. Sci.*, 2024, **42**, 1888–1896.

37 N. Chen, Y. Jin, H. Liu, C. Hu, B. Wu, S. Xu, H. Li, J. Fan and Y. M. Lee, *Angew. Chem., Int. Ed.*, 2021, **60**, 19272–19280.

38 W. Yuan, X. Zheng, X. Zhang, J. Wang, Q. Liao and Z. Wei, *J. Membr. Sci.*, 2025, **717**, 123661.

39 M. G. Marino and K. D. Kreuer, *ChemSusChem*, 2015, **8**, 513–523.

40 G. P. Dennis, K. E. O'Harra, X. Liu, E. M. Jackson, C. H. Turner and J. E. Bara, *RSC Appl. Polym.*, 2023, **1**, 111–122.

41 J. Huang, X. He, Q. Li, W. Zhang, S. Liao, C. Xiao, W. Ke, L. Zha and D. Chen, *J. Appl. Polym. Sci.*, 2025, **142**, e57202.

42 R. Selhorst, J. Gaitor, M. Lee, D. Markovich, Y. Yu, M. Treichel, C. O. Gallegos, T. Kowalewski, L. F. Kourkoutis, R. C. Hayward and K. J. T. Noonan, *ACS Appl. Energy Mater.*, 2021, **4**, 10273–10279.

43 T. Karino, Y. Ikeda, Y. Yasuda, S. Kohjiya and M. Shibayama, *Biomacromolecules*, 2007, **8**, 693–699.

44 H. Zhang, T. Wang, Y. Wang, H. Wei and W. You, *J. Membr. Sci.*, 2025, **735**, 124546.

45 B. Zhao, Z. Zhang, J. Zhang, L. Wang, T. Wang, J. Dong, C. Xu and J. Yang, *Polymer*, 2023, **286**, 126404.

46 N. Chen, J. H. Park, C. Hu, H. H. Wang, H. M. Kim, N. Y. Kang and Y. M. Lee, *J. Mater. Chem. A*, 2022, **10**, 3678–3687.

47 X. Wu, N. Chen, C. Hu, H. A. Klok, Y. M. Lee and X. Hu, *Adv. Mater.*, 2023, **35**, 2210432.

48 Z. C. Li, L. Q. Wang, H. Lee, J. Du, T. Tang, G. H. Ding, R. Ren, W. L. Li, X. Cao, S. W. Ding, W. T. Ye, W. X. Yang and L. C. Sun, *Nat. Catal.*, 2024, **7**, 944–952.